ACS APPLIED POLYMER MATERIALS

Article

Cite This: ACS Appl. Polym. Mater. 2019, 1, 160−168

pubs.acs.org/acsapm

Melt Spinning of Cellulose Nanofibril/Polylactic Acid (CNF/PLA) Composite Fibers For High Stiffness

Caitlyn M. Clarkson,[†] Sami M. El Awad Azrak,[†] Reaz Chowdhury,[†] Shoumya Nandy Shuvo,[†] James Snyder,[§] Gregory Schueneman,[‡] Volkan Ortalan,[†] and Jeffrey P. Youngblood*[,†]

[†]School of Materials Engineering, Purdue University, West Lafayette, Indiana 47907, United States of America

[‡]Forest Products Laboratory, Madison, Wisconsin 53726, United States of America

[§]Army Research Laboratory, Adelphi, Maryland 20783, United States of America

Supporting Information

ABSTRACT: Nanocellulose has potential as a reinforcing agent to improve stiffness and strength in polymer fiber; however, the inherent difference in hydrophilicity makes it challenging to incorporate it into nonhydrophilic polymers, and the composite properties are strongly anisotropic. In the present work, a dual approach was employed to incorporate cellulose nanofibrils (CNFs) into polylactic acid (PLA). Polyethylene glycol (PEG) acted as a compatibilizating agent to enable the melt spinning of CNF/PLA composite fibers without water/solvent, and CNFs were surface modified to improve compatibility, increase nanoparticle thermal stability, and increase CNF dispersion in PLA. While no significant difference was observed in strength, the stiffness improved up to 600% (1.3 wt % CNF, maximum draw) in the composite fibers. This improvement was correlated with the crystallinity and fiber orientation (Herman's order parameter) for as-spun and hot-drawn fibers.

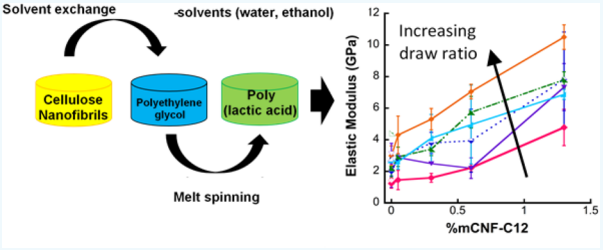

KEYWORDS: *polylactic acid, processing, melt-spinning, nanocellulose, CNF, nanocomposites*

INTRODUCTION

Nanocellulose has been explored as a reinforcement in polymer composites to provide remarkable improvement in stiffness and strength.[1−8] Applications in packaging, electronics, and fiber technology are just a few places these materials are being implemented.[9] Widespread application of nanocellulose is owing to its unique set of properties, such as high axial stiffness (78−143 GPa),[9] strength (0.2−1 GPa),[9] as well as low hydroscopic strain,[10] and low coefficient of thermal expansion.[11] Researchers have demonstrated that cellulose nanocrystals (CNCs) and cellulose nanofibrils (CNFs) both exhibit mechanical reinforcement in polymer systems, such as polylactic acid (PLA), poly(vinyl alcohol) (PVA), cellulose acetate (CA), alginate, poly(ethylene oxide) (PEO), and polyacrylonitrile (PAN).[1−3,6,12−15] CNCs are rod-like nanoparticles with dimensions of 3−5 nm wide and 20−50 nm long and crystallinity of >54%.[9] CNFs have dimensions of 4−20 nm and 0.5−2 μm and typically have a crystalline content lower than that of CNCs.[9] CNFs show improvement at small concentrations compared to CNCs despite having a lower axial stiffness due to strong entanglements and a large aspect ratio.[14] CNCs and CNFs are both highly anisotropic, and the properties of the composite depend on nanocellulose orientation as well as concentration.

Fiber applications requiring high stiffness and strength but low density may benefit from the development of nanocellulose/polymer composites because both components are low density (nanocellulose 1.5 g/cc, polymers 1−1.5 g/cc) and, as shown in previous literature, nanocellulose can increase the stiffness and strength by over 100%.[1,2,13,14] High strength, high stiffness fiber could replace materials such as fiberglass but at lower density, and, thus light-weighting components along with other environmental benefits as nanocellulose can be renewably sourced.

Cellulose nanocomposite fibers have been produced by solution-based spinning or melt spinning. Industrially, solution-based fiber spinning processes are primarily used where melt spinning processes are not otherwise possible. Polymers where the end properties justify the increased cost, time, and chemical hazards, such as Kevlar, are produced this way. Many researchers have investigated using solution-based spinning techniques to produce nanocellulose composite fibers. For instance, solution methods have been used to produce PVA/CNC fiber,[2] PVA/CNC fiber mats,[16] PVA/TEMPO−CNF fiber,[17] cellulose acetate/CNC fiber,[1] CNC/PLA fiber,[6] CNC or CNF/alginate fiber mats,[13] and CNC/PAN fiber.[3,18] These studies have demonstrated the significance of good matrix/reinforcement compatibility as well as orientation. Achieving orientation is crucial because highly oriented nanofibrils resulted in more effective stress transfer and

Received: October 17, 2018
Accepted: December 20, 2018
Published: December 20, 2018

DOI: 10.1021/acsapm.8b00030
ACS Appl. Polym. Mater. 2019, 1, 160−168

subsequently better mechanical properties.[2] Melt spinning is a simpler and cheaper process than wet- or dry-spinning and is used industrially to produce materials like nylons and polyesters which are ubiquitous. Although melt processes have been used to produce bulk materials like CNC/PLA,[19,20] CNF/PLA,[4] and CNC/PLA fibers,[5,21,22] there are few examples of melt-spun fiber, and of those, none are CNF composite fibers.[23]

Melt-spun nanocellulose/polymer composite fibers have challenged researchers for several reasons, including nanocellulose agglomeration and low thermal stability. Common approaches to address these challenges include direct liquid feeding of the nanocellulose/water solution into the polymer melt or working with the freeze-dried material; these methods have been performed with some success for bulk plastic and film.[20,23] However, agglomeration can still be present in either case.[4,23] Ideally, water should not be introduced as it plasticizes many polymers and can cause molecular weight degradation. Moreover, many polymers are processed above the thermal degradation temperature of nanocellulose. Processing over 250 °C, and sometimes much lower depending on conditions, can cause yellowing or browning of the material and property loss due to oxidation.[24−26]

Compatibilization also helps alleviate issues associated with agglomeration and thermal stability of nanocellulose. A wide variety of surface functionalization methods have been developed for attaching fatty acids, plasticizers, and small functional groups and ions (carboxylic acid, sulfate, phosphate) to make nanocellulose more compatible with hydrophobic media.[27−31] Surface modification can help shield or eliminate hydrogen bonding between neighboring particles or change the hydrophobicity of nanocellulose. Thermal stability also generally improves with modification. These methods are common for making nanocellulose/PLA composites as there is an inherent difference in hydrophilicity between the matrix and reinforcement.[29,32−35] In addition to changing the nanoparticle surface, polymer systems have been made more compatible by the addition of plasticizers like polyethylene glycol (PEG)[36] or glycerol triacetate[20] to PLA. Although plasticizers are uncommon in fibers, they may impart additional benefits, such as improving drawing or reducing embrittlement (commonly seen in nanocellulose composites).

PLA has generated interest because it is renewably sourced, industrially biocompostable, and has environmental benefits like low CO_2 emissions during production. It has applications in 3D printing filament, bioabsorbable/biodegradable materials for medicine, fibers and nonwovens in domestic products, and food packaging. Nanocellulose/PLA composites primarily aim to improve the mechanical properties of PLA (which are generally inferior to other polyesters and nylon) or the crystallization rate. There is extensive evidence that nanocellulose can do both.[5,6,20,22,33−35] Additionally, PLA has a relatively low melting point (150−170 °C) which allows for reduced processing temperatures.

The present study reports surface-modified CNF/PLA composite fibers by continuous melt spinning. To achieve this goal, CNF were chemically modified (mCNF) using a method developed previously by Yoo et al.[27] to improve nanoparticle/polymer interactions, which affect mechanical performance. Additionally, a compatibilizer was selected to carry the modified mCNFs into PLA. There are several reasons PEG was chosen. First, PEG is a miscible, known plasticizer for PLA. Second, mCNFs could be exchanged into PEG; this reduced potential molecular weight degradation by hydrolysis of PLA with water. Lastly, at low concentrations, low molecular weight PEG should not phase separate, but can increase the ductility of PLA.[37,38] Since mechanical performance also is strongly affected by nanoparticle alignment, fibers were hot-drawn post-fabrication. Mechanical properties were correlated to crystallinity and orientation with use of differential scanning calorimetry (DSC) and wide-angle X-ray spectroscopy (WAXS).

METHODS

Materials. Mechanically fibrillated CNF was acquired from the University of Maine, Orono, ME, USA (Lot # U22; 3% CNF-water slurry; 90% fines). PEG was purchased from Sigma-Aldrich, St. Louis, MO, USA (M_n = 600g/mol). Nature Works INGEO-3001D polylactic acid was purchased from Jamplast, Ellisville, MO, USA. The CNFs were chemically modified through the hydroxyl group on the nanoparticle surface using methods outlined in Yoo et al.[27] The process produced nanoparticles grafted with PLA and capped with a 12-carbon aliphatic chain, as shown in the schematic in Figure 1B.

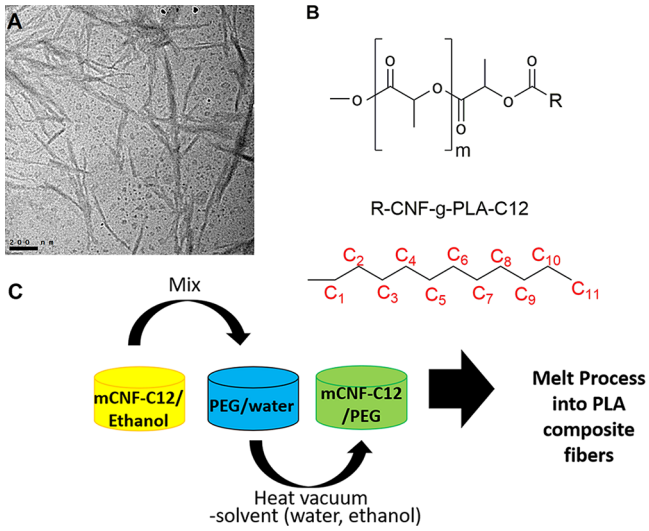

Figure 1. (A) TEM micrograph of mCNF-C12 cast from PEG/water. (B) Schematic of surface modification on CNF surface. (C) Process of exchanging mCNF-C12 into PEG to melt process into PLA.

Chemically modified CNF (mCNF) is referred to as mCNF-C12 henceforth. The modified product was approximately 8.5% mCNF-C12 in ethanol (EtOH) after modification; Fourier transform infrared spectroscopy (FTIR) data is shown in Figure S6, confirming formation of the ester. Thermogravimetric analysis (TGA) confirmed that the onset of thermal degradation temperature was slightly improved after modification despite the reduction in particle size (Figure S7).Chemical modification allowed higher CNF concentrations to be achieved in the PEG solutions as higher than 2 wt % of unmodified CNF in PEG could not be easily achieved. Nanoparticle morphology was characterized with transmission electron microscopy (TEM); a side-by-side comparison of before and after chemical modification is in Figure S1.

To prepare final PEG/mCNF-C12 solutions at 1, 5, 10, and 20 wt % mCNF-C12, an EtOH/water-based solution was made from solutions of PEG dissolved in water and mCNF-C12 in EtOH. A Branson Ultrasonifyer was employed to disperse mCNF-C12 into the EtOH at 30% amplitude with a 1 s pulse and 1 s off for a maximum of 30 s. The solutions were combined by first mechanically mixing and then ultrasonification. To remove the solvent, a vacuum oven with a liquid nitrogen cooled solvent trap was employed. The temperature of

DOI: 10.1021/acsapm.8b00030
ACS Appl. Polym. Mater. 2019, 1, 160−168

the vacuum oven was 70 °C and 5−10 in-Hg. This process is visually represented in Figure 1C.

Melt Spinning and Post-Processing. A twin-screw Xplore 5 cc microcompounder with a 90° turn and 1 mm orifice was used to produce melt spun composite fibers at 200 °C and a 50 rpm rotary screw speed. Fibers were collected directly from the orifice on a Randcastle winding mandrel running at 150 rpm. PLA pellets were dried at 100 °C overnight to remove absorbed water prior to compounding. The PEG/mCNF-C12 solutions were measured to produce composite fibers at concentrations of 0.05, 0.3, 0.6, and 1.3 wt % mCNF-C12 from prepared solutions. Half of the material was first loaded through a continuous feed hopper, then the plasticizer was injected, and the remaining material was added again through the continuous feed hopper. The total compounding process was approximately 2.5 min, with 1.5 min of compounding the material after loading, during which material can be recirculated through the compounder. Materials were compounded in sequential order with the transition material being disposed of between concentrations. The concentration of PEG was constant at 5 wt %. As a control, 0 wt % PEG 0 wt % mCNF-C12 fibers were also produced. Hot-drawing was performed over a 100 °C heated parallel plate system by hand to draw ratios, L/L_0, up to six times the original length of the fiber, which was 25.4 mm initially. A change in birefringence was observed with hot drawing, and representative images can be found in Figure S2.

Morphology and Dispersion. Fiber morphology was analyzed across multiple scales, optical microscopy (OM) and scanning electron microscopy (SEM). OM images of as-spun fibers and hot-drawn fibers were taken on a Carl Zeiss (Axio observer A1) inverted light microscope equipped with a linearly polarized light filter. Fiber morphology was imaged using an XL40 field emission SEM. Sample surfaces were sputter coated with a conductive gold−palladium barrier to help relieve charge built up on the polymer surface. Instrument parameters were 3−5 keV accelerating voltage and a working distance of 14−20 mm.

TEM images were taken before and after chemical modification of the mechanically fibrillated CNF, as chemical modification can change nanoparticle morphology. A 0.5 wt % mCNF-C12 solution was prepared by mechanically mixing the appropriate amount of mCNF-C12 from EtOH with 10 mL of deionized water, with less than 10 ppb total organic carbon (TOC) made in-house. The solution was then ultrasonicated using a Branson Ultrasonifyer for 30 s at 30% power amplitude. Afterward, two drops of the sample mixture solution were drop-casted on a 200-mesh copper grid with an amorphous carbon support membrane and were dried overnight in a sealed container to avoid any contamination before they were placed in the TEM holder the next day. BF-TEM images were taken at 300 kV on a FEI Titan ETEM 80−300 equipped with a Gatan Tridiem GIF without staining the sample with any staining agent. Several images at different regions of the samples, both in low and high magnification, were taken to fortify the data statistics.

Crystallinity and Orientation. Thermal properties of as-spun and hot-drawn fibers were determined on a Thermal Analysis (TA) Q2000 DSC. Heating experiments were performed at 10 °C/min on hermetically sealed aluminum pans in a nitrogen atmosphere. DSC experiments are on multiple fibers, which were bundled into a "hair-ball" and then sealed in the pan. Sample mass was approximately 7 ± 2.5 mg.

The order parameter, S, is a measure of the orientation. In nanocellulose and its composites, S has been primarily measured by WAXS.[1,2,39−41] However, alternative methods, such as the determination of alignment from birefringence, also exist.[42,43] Optical methods can offer significant advantages over conventional X-ray spectroscopy in terms of cost and capability. Therefore, WAXS measurements were compared to measurements made using an OM-birefringence method. Methods for each measurement are subsequently provided.

For orientation experiments, samples were prepared by carding for ease of handling and transport. In brief, a 3 mm × 5 mm rectangular hole was cut from the center of thick cardstock. Three to five fibers were carefully glued parallel to each other and mounted in the WAXS such that the fiber axis was parallel to the source. The OM method used the same samples.

Estimation of the order parameter from OM images was performed using ImageJ and a Carl Zeiss (Axio observer A1) inverted light microscope equipped with a linearly polarized light filter. Two images were taken at 0° and at 45° after finding the maximum intensity. Using ImageJ software, the mean pixel intensity and background intensity of the images were measured. Details can be found in the Supporting Information. S can be calculated from eq 1[42]

$$S = \frac{D - 1}{D + 2} \tag{1}$$

where $D = I_{45}/I_0$, and $I_{45\ \text{or}\ 0} = I_{\text{Fiber}} - I_{\text{Background}}$.

Orientation in composite fibers was also measured by WAXS. The fibers were tested in transmission mode using a Cu Kα beam with a wavelength (λ) of 0.154 nm and a sample to detector distance of 79.248 mm. The equipment used was the SAXSpoint 2.0 (Anton Paar), equipped with a Dectris R1M photon counting hybrid pixel detector and a single crystal silicon scatter-less slits collimation tube. The detector was mounted on a tilted configuration to achieve wide-angle X-ray diffraction (up to $2\theta = 60°$). Due to equipment limitation, half of the scattering pattern was available. Samples were mounted on cardboard for ease of handling and to facilitate easier alignment by mounting the fiber parallel to the short axis.

Fibers were irradiated for a total of 1000 s (4 intervals of 250 s each). Using the supplied software, the obtained 2D scattering patterns were converted to 1D scatter plots ($I(\theta)$ vs 2θ), and background noise (cosmic radiation) was subtracted from all curves. Each curve was then normalized to the minimum intensity value to compare across all fiber scatter intensities. To obtain the Herman's order parameter (S), the $I(\phi)$ vs azimuthal angle distribution was used. These distributions were generated by radial integration of the 2D scatter plots at a 2θ of 16 ± 0.1°, which represented the PLA (200) plane/peak. Thus, the order parameter can be calculated as follows:[44,45]

$$S = \frac{1}{2}(3\langle \cos^2 \phi_{200,Z}\rangle - 1) \tag{2}$$

$$\langle \cos^2 \phi_{200,Z}\rangle = \frac{\sum_{0°}^{180°} I(\phi)\sin(\phi)\cos^2\phi}{\sum_{0°}^{180°} I(\phi)\sin(\phi)} \tag{3}$$

As described by Alexander and developed by P.H. Herman and his co-workers, because the fibers have been drawn to some degree and some of the crystal domains align with the fiber axis, this method can be used as a direct measure of crystallinity order with respect to the fiber axis.[44,45] In this case, total alignment represents a value of $S = 1$, and completely random orientation has a value of $S = 0$[1]. Similarly, other researchers have used this technique to find the order parameter of alginate nanocomposite fibers.[39]

Tensile Properties. The mechanical performance of as-spun and drawn fibers were quantified using a TA Instruments Q800 dynamic mechanical analyzer (DMA). Stress/strain experiments were performed using a force ramp at 0.3 N/min and 0.001 N preload; the temperature was 23 °C and 30% relative humidity. Sample preparation followed the procedure outlined in Clarkson et al.[6] The actual gauge length and minimum diameter of the fiber were recorded for calculation of the engineering stress and engineering strain from optical microscopy images taken prior to testing the sample. The sample size was 2−4 samples per condition, and error bars are one standard deviation.

RESULTS AND DISCUSSION

Nanoparticle Morphology. The modification process produced nanoparticles with a very different morphology than the unmodified mechanically fibrillated CNF (Figures 1A and S1). Notably, the mCNF-C12 is shorter and thinner (thickness = 26.2 ± 9.6, length= 384.5 ± 109.7). In the unmodified CNF, entanglements appeared to be very long-range (>500 nm), and

DOI: 10.1021/acsapm.8b00030
ACS Appl. Polym. Mater. 2019, 1, 160−168

particles exhibited fibrillated structure. The mCNF-C12 still exhibit evidence of entanglements; however, there are now individual, small mCNF-C12s. Theoretically, the surface modification process could have broken down the amorphous regions of the CNFs, while the stronger, more crystalline regions would have been left behind.

Surface Morphology. Microscopic evidence of increased surface roughness with mCNF-C12 concentration is evident in Figure 2A,B. Ideally, individual nanoparticles would be homogeneously dispersed in the matrix; however, mCNF-C12 networks, which are entangled and long, are nearly impossible to completely break up during compounding, regardless of chemical modification of fibrils and high shear rates. Despite ultrasonication of the mCNF-C12 solutions prior to solvent exchange, there is evidence of pre-existing entanglements of mCNF-C12s in the TEM image (Figure 1 A) of mCNF-C12 in PEG, which would have been carried over into the compounding process. Instead, these nanoparticles may be distributed throughout the matrix in a mixture of pre-existing entanglements and individual mCNF-C12s. There is some evidence of larger microscopic agglomerations in Figures 2E,F and S2; however, the submicron bumps appear to be uniformly distributed throughout the fibers.

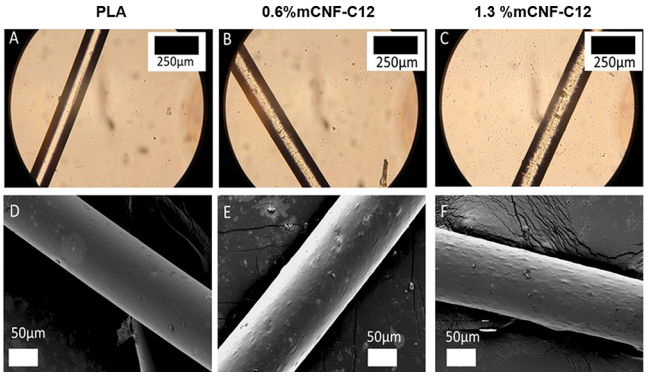

Figure 2. (A–C) Optical micrographs at select concentrations of mCNF-C12. (D–F) SEM images showing surface morphology with the addition of up to 1.3 wt % mCNF-C12.

Crystallinity. Crystallinity can be an essential component in obtaining good mechanical performance; however, PLA is a slow crystallizing polymer and does not usually obtain high degrees of crystallinity during rapid processing. Nevertheless, crystallization can be driven by the addition of various additives (such as nucleation agents) as well as through post-processing (hot-drawing).[2,22,32,33] DSC was employed to measure the thermal properties of the composite fibers before and after hot-drawing and with increasing mCNF-C12 content (fixed PEG content). The thermal properties have been tabulated in Table 1 for DSC thermograms of three thermal histories. As many fibers had to be hand drawn to produce a sufficient sample for DSC, the values represent an average of the material's thermal properties. The degree of crystallinity, χ, was calculated with eq 4, where ΔH_m°, the theoretical maximum melting enthalpy of PLA, is 93 J/g, and x is the weight fractions of mCNF-C12 and PEG in the composite fibers.[21,22,37,46,47] The enthalpies of cold crystallization and experimental melting enthalpy are ΔH_{cc} and ΔH_m, respectively. Details for these measurements can be found in the Supporting Information.

$$\chi\% = 100\%(\Delta H_m + \Delta H_{cc})/(\Delta H_m^\circ(1 - x_{CNF+PEG})) \quad (4)$$

During reheating in the DSC, the material can undergo further crystallization, and a cold crystallization peak can be observed. The DSC thermograms (Figure 3A) show the cold crystallization peak over 85–100 °C, which is a consequence of the slow crystallization of PLA and is typically observed; also observed is an enthalpic peak immediately before the melting endotherm. This peak is most commonly associated with the formation of the less ordered α' phase reordering at high temperature. With the addition of mCNF-C12, these peaks are

Table 1. Thermal Properties for Three Thermal Histories

DR	%PEG	%mCNF-C12	T_g (°C)	T_{cc} (°C)	T_m (°C)	ΔH_{cc} (J/g)	ΔH_m (J/g)	X (%)
				As-spun				
0	0	0	63.1	95.1	169.0	31.1	34.6	3.8
0	5	0	50.0	79.1	165.6	28.9	35.7	7.8
0	5	0.05	52.3	82.9	166.9	27.0	35.7	9.8
0	5	0.3	56.5	85.8	166.5	28.6	37.5	10.2
0	5	0.6	56.8	83.4	166.4	23.8	32.1	9.4
0	5	1.3	58.4	88.0	166.7	26.4	31.7	6.1
				Intended DR: 3×				
3	0	0	64.6	64.5	98.8	10.9	42.4	33.8
3	5	0	49.3	71.6	162.9	8.2	26.0	20.1
3	5	0.05	45.2	84.2	164.5	10.3	33.2	25.9
3	5	0.3	55.6	85.1	164.9	22.6	39.6	19.3
3	5	0.6	58.2	75.5	167.1	13.1	36.1	26.2
3	5	1.3	58.5	87.5	165.7	2.7	27.9	28.5
				Maximum Draw				
4	0	0	63.1	102.2	168.4	10.7	44.8	36.6
6	5	0	47.9	80.6	164.1	8.8	43.6	39.4
6	5	0.05	52.7	82.8	164.7	6.6	30.7	27.3
6	5	0.3	56.1	85.7	164.9	7.2	37.2	34.0
6	5	0.6	53.6	85.0	164.6	5.6	30.6	28.5
6	5	1.3	58.3	86.6	165.9	6.4	36.7	34.7

DOI: 10.1021/acsapm.8b00030
ACS Appl. Polym. Mater. 2019, 1, 160–168

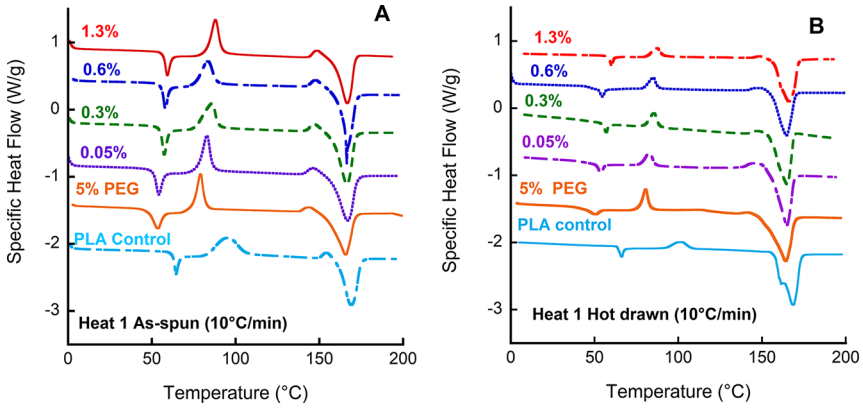

Figure 3. DSC thermograms of (A) as-spun PLA composite fibers and (B) composites fibers at the maximum hot-draw ratio (6× for all but PLA control, which was 4×).

still present; however, the cold crystallization peak temperature (T_{cc}) (Table 1) is observed to shift to lower temperatures, and the cold crystallization peaks generally appear sharper compared to neat PLA. Additionally, the glass transition temperature (T_g) is suppressed to lower temperatures which can be indicative of a higher initial crystallinity. Although molecular confinement of amorphous regions by mCNF-C12 or addition of 5%PEG from the PLA crystal structure may also account for the decrease in T_g observed. Exploration of low-molecular weight PEG as a plasticizer has shown that PEG may decrease T_g by up to 15 °C at low concentrations.[37] A melting endotherm at 15−25 °C was not observed in any DSC thermogram, indicating that at 5% PEG, there was no phase separation. This is in good agreement with the literature for low molecular weight PEGs in PLA over the 200−1000 g/mol range.[37,38] By accounting for the cold crystallization during heating in the DSC, a relative value of the crystallinity, χ, from the fiber processing history can be obtained from eq 4.

Generally, the as-spun fibers all exhibited low degrees of crystallinity, since, during processing, the fiber line experiences rapid cooling. However, at very small concentrations of 0.05 and 0.3 wt % mCNF-C12, χ was observed to increase from 3.8% for neat PLA to a maximum of 10.2% crystallinity, which suggests that at small concentrations, the mCNF-*g*-PLA-C12 is a good heterogeneous nucleation agent (Table 1). Above 0.3%, the as-spun χ values began to decrease, presumably because of mCNF-C12 percolation inhibiting molecular rearrangement, which has been observed in other systems.[2,6,48]

During hot-drawing, the material has a second chance to crystallize. The hot-drawing temperature was 100 °C, which is just above the cold crystallization temperatures for all as-spun samples. For fibers hot-drawn to 3× the original fiber length, χ increased compared to the as-spun conditions, but all fibers obtained χ of ∼20% or greater, with a maximum of 33.8% (PLA). Further hot-drawing did not produce a substantial increase in χ, as most values remained the same, except for the 5% PEG and the 0.3%mCNF-C12, which were improved. Variation in these samples due to preparation might result in the difference observed in the 3× draw ratio and maximum draw ratio. Additionally, the hot-drawn fibers still exhibited cold crystallization upon heating in the DSC; although the cold crystallization peaks largely decreased after hot-drawing compared to the as-spun material. Since the degree of crystallinity is similar across hot-drawn samples, this alone cannot account for mechanical performance. The other factors which will potentially effect performance are mCNF-C12 concentration as well as alignment.

Orientation. The orientation of the polymer and nanoparticles along the fiber axis is equally important in determining mechanical performance. As nanocellulose is highly anisotropic, maximizing the mechanical performance necessitated further alignment during hot-drawing, and consequently, alignment of the polymer chains along the fiber axis has a similar effect. The orientation was measured using WAXS for three thermal histories (as-spun, 3×, and maximum draw) and is shown in Figure 4. WAXS diffractions

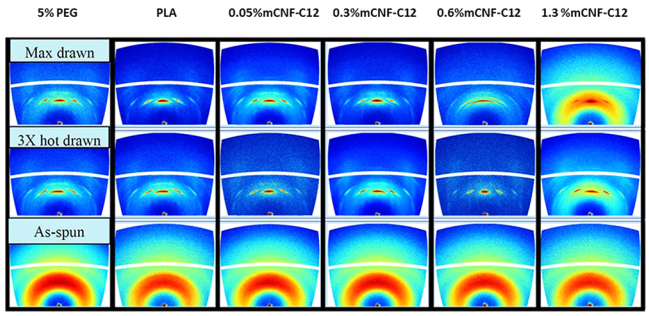

Figure 4. 2D WAXS diffraction patterns for three thermal histories.

patterns show an amorphous halo in the as-spun fibers, and as fibers are hot-drawn; diffraction peaks appear due to increased crystallinity and alignment with hot-drawing. The Herman's order parameter was calculated using eqs 1 and 2 from the 2D diffraction patterns. Although PLA and CNF have (200) peaks at similar 2ϕ, at such small concentrations of mCNF-C12, the WAXS patterns observed are effectively only for PLA. The 1D patterns, which were extracted from 2D plots, show only peaks corresponding to PLA and no evidence of nanocellulose (Supporting Information S3).

Herman's order parameter (S) is plotted in Figure 5A. Initially, S is less than 0.1 (unordered) since the as-spun fibers possess low crystallinity and low alignment. After hot-drawing, S increased to 0.65−0.75 (highly ordered) up to 0.6 wt % mCNF-C12, in the case of 3×, and up to 0.3 wt % mCNF-C12 for the maximum hot-draw. Above 0.3 wt % mCNF-C12, the order parameter decreases with increasing mCNF-C12 concentration and with increasing draw ratio. This may be because of molecular confinement at higher mCNF-C12 concentrations. A potential explanation is shown in Figure

DOI: 10.1021/acsapm.8b00030
ACS Appl. Polym. Mater. 2019, 1, 160−168

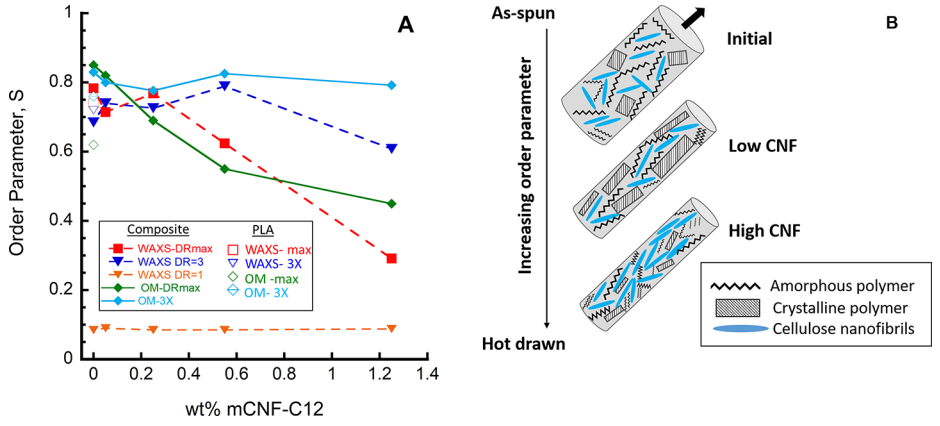

Figure 5. (A) Herman's order parameter effect of hot-drawing and mCNF-C12 content at a constant PEG content of 5% (dotted lines are unmodified PLA) and (B) visualization of the effect of hot-drawing on fibers with low mCNF-C12 and high mCNF-C12 content.

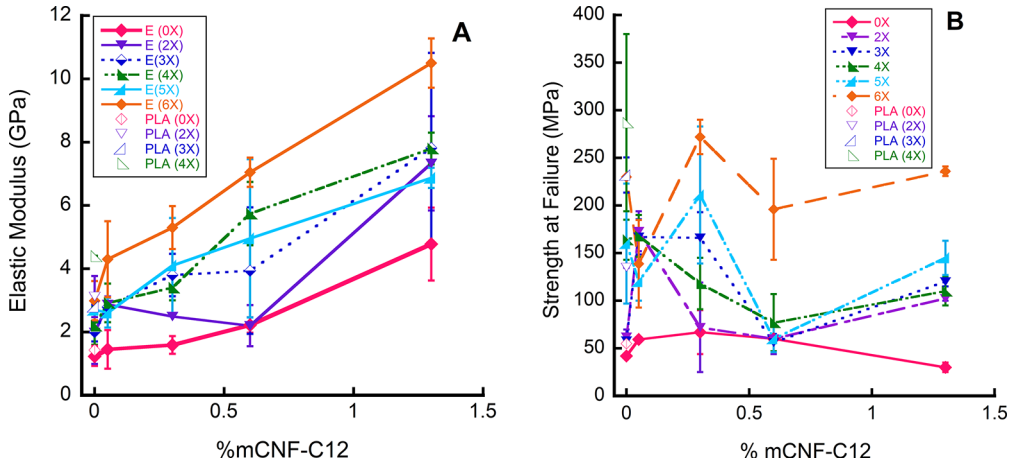

Figure 6. (A) Elastic modulus vs mCNF-C12 content and (B) strength-at-failure vs mCNF-C12. The 0% mCNF-C12 refers to fibers with 5%PEG, and the PLA without any additives is shown as individual points (legend for details).

5B. Initially, all fibers are comprised of mCNF-C12, amorphous and crystalline polymer, and free/unoccupied volume. The molecules are not highly ordered in this state. As the fiber is hot-drawn, the unoccupied volume is reduced, and the polymer can crystallize (resulting in additional densification). In the case of the low concentration, there are few mCNF-C12 to act as physical barriers, and so, the amorphous and crystalline polymer can be aligned along the fiber axis during drawing. However, at high concentration, the mCNF-C12 occupy a larger volume in the sample. Drawing of the fiber will bring nanoparticles closer together to the point where a percolation network is formed (if it did not already exist to some extent). Consequently, aggregation or molecular confinement may also impede crystallization (in addition to PLA alignment), this does not appear to be the case, as observed in Table 1 (constant crystallinity), for the hot drawn fibers. Although *S* of PLA is decreasing, the nanoparticles may still be aligned along the fiber axis; however, above a certain concentration, CNF alignment will also reach a maximum. Unfortunately, at small concentration of CNF, WAXS cannot be used to determine the order of mCNF-C12

S was also calculated from OM-birefringence, and *S* values are shown in Figure 5A as well. Comparison of these two data sets is on a trend basis only, as the techniques probe different levels of the fiber structure. WAXS measures the crystalline orientation, while optical methods also capture the amorphous contribution to orientation and can be used to probe orientation at a smaller local scale. For the *S* estimations in this study, intensity was measured for a large area to be more comparable to the bulk properties measured by WAXS. There are some qualitative similarities to the WAXS data. Like the WAXS, *S* is high at low concentration for both the 3× and maximum draw ratios; however, *S* deviated at a different concentration compared to the WAXS (0.3 wt % compared to 0.6 wt %). Additionally, *S* of the 3× did not decrease at 1.3 wt % for the OM-data like it did for the WAXS measurements. Deviation in *S* between WAXS and OM-birefringence could be due to several sources, such as small errors in alignment during imaging of the fibers in the 0° and 45° positions and measuring and the contribution of amorphous order.

Mechanical Performance. Tensile tests were conducted on single fibers. The elastic modulus and strength at failure are reported in Figure 6A,B (Table S1). Addition of 5% PEG to PLA produced an initial decrease in elastic modulus and strength, which is in good agreement with other studies that explored low molecular weight PEG as a plasticizer for PLA.[37,38] The elastic modulus was observed to depend strongly on mCNF-C12 content and on processing history. In the as-spun fibers, the modulus was observed to increase with increasing mCNF-C12 content; however, the improvements were small until 1.3 wt %, in which the elastic modulus went from 1.4 to 4 GPa (up to 10.5 GPa with hot-drawing for

DOI: 10.1021/acsapm.8b00030
ACS Appl. Polym. Mater. 2019, 1, 160−168

1.3 wt % mCNF-C12). The as-spun fibers exhibited low orientation (Figure 5A) and low to moderate crystallinity (Table 1), which suggests that mCNF-C12 content alone is primarily responsible for the increase in stiffness. The strength at failure data of the as-spun fibers appears to remain constant, while at higher concentrations and draw-ratios, the incidence of random failure during mechanical testing became more prevalent, as a transition from more ductile-like behavior to brittle-like behavior was observed; this coincided with a transition in fracture type (Figure S4). Fibers may also have failed prematurely because of defects in the samples, such as variation in fiber diameter or agglomerations/entanglements like those in Figure S2, which were not apparent in as-spun fibers until after drawing.

Several factors can affect the elastic modulus, crystallinity, alignment, and concentration. After hot-drawing, all fibers exhibited approximately the same degree of crystallinity; therefore, orientation and concentration are suggested to be the primary factors affecting differences in the stiffness. Hot-drawing was performed to facilitate alignment of both the polymer and mCNF-C12 along the fiber axis and was observed to improve the elastic modulus of both 0 wt % as well as composite fibers. From the as-spun state to the maximum hot-draw, stiffness improved over 200% for all conditions. Although S increased with hot-drawing, it did not exhibit the same monotonic dependence as the stiffness data. It increased substantially in neat PLA and at low concentrations of CNF, and then at or above 0.6 wt % mCNF-C12, it exhibited increasing disorder both as CNF concentration increased and draw ratio increased. Despite achieving similar χ and decreasing S parameter, the elastic modulus is highest for the maximum draw and at the highest concentrations of mCNF-C12, which suggests a strong dependence on concentration and implies that the mCNF-C12 are being preferably aligned along the fiber axis even though the polymer may be molecularly confined. Upon examination of Figure 6, from the as-spun 0−1.3 wt %, the stiffness increase is primarily a function of increased concentration of the stiffer mCNF-C12 nanoparticles; however, with hot-drawing, the stiffness can be further increased, presumably by the alignment of stiffer axis of the mCNF-C12 particles along the fiber axis. Smaller draw ratios exhibit similar qualitative behavior, although inconsistent processing of these fibers may have produced more variability in stiffness.

At the maximum DR, the strength at failure of the mCNF-C12 composites was approximately the value of the PLA. Although there are several confounding factors in the strength at failure data, an important factor is the reduction of the orientation parameter with increasing concentration of mCNF-C12 and draw ratio. At higher DR, the polymer components are trapped by the mCNF-C12 network and will not be aligned along the tensile axis, and thus, the contribution to the strength from the PLA matrix may be less than the composite fibers with lower concentration and at smaller DR. Moreover, the strength at failure of the composite will depend in part on the strength at failure of the individual components. Celluloses exhibit a strength at failure in the range of 200−1000 MPa.[9] The strength at failure of the mCNF-C12 used in the present study may be similar to those previously reported, since nanocellulose is comprised of cellulose I and cellulose II. However, due to the brittle behavior exhibited by the neat PLA and composite fibers, it is difficult to distinguish between the role of alignment, CNF concentration, and defect presence.

CONCLUSIONS

In the present study, a method to continuously melt spin mCNF-C12/PLA composite fibers without the introduction of water or solvent into the compounder was assessed. Composite fibers were produced by solvent exchanging modified CNF into PEG at various concentrations and melt blending into PLA. This method allowed very small concentrations of CNF (0.05 wt %) to be achieved and relatively high concentrations (1.3 wt %) as well. At high concentrations, there is some evidence that pre-existing entanglements or agglomerations of the mCNF-C12 were not removed during compounding; although dispersion appears good otherwise. Fibers were hot-drawn to facilitate alignment of the polymer matrix and mCNF-C12, which are highly anisotropic.

Despite the use of plasticizer as a processing aid and compatibilizer, the stiffness of the composite fibers was improved. The stiffness increased 280% for the as-spun fibers and 600% with hot-drawing. The strength at failure was scattered due to the embrittlement of the composite fibers with mCNF-C12 as well as agglomerations or entanglements acting as defects in the fiber. mCNF-C12 concentration appears to be the dominant factor in the improvement in stiffness as the hot-drawn fibers achieved similar degrees of crystallinity, and orientation (of the polymer) was observed to decrease at high mCNF-C12 concentrations.

ASSOCIATED CONTENT

Supporting Information

The Supporting Information is available free of charge on the ACS Publications website at DOI: 10.1021/acsapm.8b00030.

Transmission electron microscopy images before and after chemical modification, optical microscopy images of birefringence, additional X-ray diffraction patterns, scanning electron microscopy images of fiber fracture faces, optical microscopy showing the method for order parameter estimate from birefringence, Fourier transform infrared spectroscopy and thermal gravimetric analysis, differential scanning calorimetry analysis, and a table of mechanical properties (PDF)

AUTHOR INFORMATION

Corresponding Author

*E-mail: jpyoungb@purdue.edu; Phone: +1 765-496-2294; Fax: +1 765-494-1204.

ORCID

Caitlyn M. Clarkson: 0000-0001-9689-0842
Reaz Chowdhury: 0000-0002-8478-4222
Jeffrey P. Youngblood: 0000-0002-8720-8642

Notes

The authors declare no competing financial interest.

ACKNOWLEDGMENTS

The authors would like to acknowledge financial support from the Private-Public Partnership for Nanotechnology in the Forestry Sector (P3Nano) under Grant 107528, the Forest Products Laboratory Grant 17000384, and National Science Foundation Integrative Graduate Education and Research Traineeship: Sustainable Electronics Grant 1144843.

DOI: 10.1021/acsapm.8b00030
ACS Appl. Polym. Mater. 2019, 1, 160−168

REFERENCES

(1) Chen, S.; Schueneman, G.; Pipes, R. B.; Moon, R. J.; Youngblood, J. Effects of Crystal Orientation on Cellulose Nanocrystals − Cellulose Acetate Nanocomposite Fibers Prepared by Dry Spinning. *Biomacromolecules* **2014**, *15*, 3827−3835.

(2) Uddin, A. J.; Araki, J.; Gotoh, Y. Toward "Strong" Green Nanocomposites: Polyvinyl Alcohol Reinforced with Extremely Oriented Cellulose Whiskers. *Biomacromolecules* **2011**, *12*, 617−624.

(3) Chang, H.; Chien, A. T.; Liu, H. C.; Wang, P. H.; Newcomb, B. A.; Kumar, S. Gel Spinning of Polyacrylonitrile/Cellulose Nanocrystal Composite Fibers. *ACS Biomater. Sci. Eng.* **2015**, *1*, 610−616.

(4) Jonoobi, M.; Harun, J.; Mathew, A. P.; Oksman, K. Mechanical Properties of Cellulose Nanofiber (CNF) Reinforced Polylactic Acid (PLA) Prepared by Twin Screw Extrusion. *Compos. Sci. Technol.* **2010**, *70*, 1742−1747.

(5) John, M. J.; Anandjiwala, R.; Oksman, K.; Mathew, A. P. Melt-Spun Polylactic Acid Fibers: Effect of Cellulose Nanowhiskers on Processing and Properties. *J. Appl. Polym. Sci.* **2013**, *127*, 274−281.

(6) Clarkson, C. M.; Youngblood, J. P. Dry-Spinning of Cellulose Nanocrystal/Polylactic Acid Composite Fibers. *Green Mater.* **2018**, *6*, 6−14.

(7) Peng, S. X.; Shrestha, S.; Yoo, Y.; Youngblood, J. P. Enhanced Dispersion and Properties of a Two-Component Epoxy Nanocomposite Using Surface Modified Cellulose Nanocrystals. *Polymer* **2017**, *112*, 359−368.

(8) Gupta, A.; Simmons, W.; Schueneman, G. T.; Hylton, D.; Mintz, E. A. Rheological and Thermo-Mechanical Properties of Poly(Lactic Acid)/Lignin-Coated Cellulose Nanocrystal Composites. *ACS Sustainable Chem. Eng.* **2017**, *5*, 1711−1720.

(9) Moon, R. J.; Martini, A.; Nairn, J.; Simonsen, J.; Youngblood, J. Cellulose Nanomaterials Review: Structure, Properties and Nanocomposites. *Chem. Soc. Rev.* **2011**, *40*, 3941−3994.

(10) Shrestha, S.; Diaz, J. A.; Ghanbari, S.; Youngblood, J. P. Hygroscopic Swelling Determination of Cellulose Nanocrystal (CNC) Films by Polarized Light Microscopy Digital Image Correlation. *Biomacromolecules* **2017**, *18*, 1482−1490.

(11) Diaz, J. A.; Wu, X.; Martini, A.; Youngblood, J. P.; Moon, R. J. Thermal Expansion of Self-Organized and Shear-Oriented Cellulose Nanocrystal Films. *Biomacromolecules* **2013**, *14*, 2900−2908.

(12) Gupta, B.; Revagade, N.; Anjum, N.; Atthoff, B.; Hilborn, J. Preparation of Poly(Lactic Acid) Fiber by Dry-Jet-Wet-Spinning. I. Influence of Draw Ratio on Fiber Properties. *J. Appl. Polym. Sci.* **2006**, *100*, 1239−1246.

(13) Urena-Benavides, E. E.; Brown, P. J.; Kitchens, C. L. Effect of Jet Stretch and Particle Load on Cellulose Nanocrystal-Alginate Nanocomposite Fibers. *Langmuir* **2010**, *26*, 14263−14270.

(14) Xu, X.; Liu, F.; Jiang, L.; Zhu, J. Y.; Haagenson, D.; Wiesenborn, D. P. Cellulose Nanocrystals vs. Cellulose Nanofibrils: A Comparative Study on Their Microstructures and Effects as Polymer Reinforcing Agents. *ACS Appl. Mater. Interfaces* **2013**, *5*, 2999−3009.

(15) Xu, X.; Wang, H.; Jiang, L.; Wang, X.; Payne, S. A.; Zhu, J. Y.; Li, R. Comparison between Cellulose Nanocrystal and Cellulose Nanofibril Reinforced Poly(Ethylene Oxide) Nanofibers and Their Novel Shish-Kebab-like Crystalline Structures. *Macromolecules* **2014**, *47*, 3409−3416.

(16) Peresin, M. S.; Habibi, Y.; Zoppe, J. O.; Pawlak, J. J.; Rojas, O. J. Nanofiber Composites of Polyvinyl Alcohol and Cellulose Nanocrystals: Manufacture and Characterisation. *Biomacromolecules* **2010**, *11*, 674−681.

(17) Endo, R.; Saito, T.; Isogai, A. TEMPO-Oxidized Cellulose Nanofibril/Poly(Vinyl Alcohol) Composite Drawn Fibers. *Polymer* **2013**, *54*, 935−941.

(18) Chang, H.; Luo, J.; Liu, H. C.; Bakhtiary Davijani, A. A.; Wang, P. H.; Lolov, G. S.; Dwyer, R. M.; Kumar, S. Ductile Polyacrylonitrile Fibers with High Cellulose Nanocrystals Loading. *Polymer* **2017**, *122*, 332−339.

(19) Oksman, K.; Mathew, A. P.; Bondeson, D.; Kvien, I. Manufacturing Process of Cellulose Whiskers/Polylactic Acid Nanocomposites. *Compos. Sci. Technol.* **2006**, *66*, 2776−2784.

(20) Herrera, N.; Mathew, A. P.; Oksman, K. Plasticized Polylactic Acid/Cellulose Nanocomposites Prepared Using Melt-Extrusion and Liquid Feeding: Mechanical, Thermal and Optical Properties. *Compos. Sci. Technol.* **2015**, *106*, 149−155.

(21) Blaker, J. J.; Lee, K. Y.; Walters, M.; Drouet, M.; Bismarck, A. Aligned Unidirectional PLA/Bacterial Cellulose Nanocomposite Fibre Reinforced PDLLA Composites. *React. Funct. Polym.* **2014**, *85*, 185−192.

(22) Sullivan, E. M.; Moon, R. J.; Kalaitzidou, K. Processing and Characterization of Cellulose Nanocrystals/Polylactic Acid Nanocomposite Films. *Materials* **2015**, *8*, 8106−8116.

(23) Oksman, K.; Aitomaki, Y.; Mathew, A. P.; Siqueira, G.; Zhou, Q.; Butylina, S.; Tanpichai, S.; Zhou, X.; Hooshmand, S. Review of the Recent Developments in Cellulose Nanocomposite Processing. *Composites, Part A* **2016**, *83*, 2−18.

(24) Kargarzadeh, H.; Ahmad, I.; Abdullah, I.; Dufresne, A.; Zainudin, S. Y.; Sheltami, R. M. Effects of Hydrolysis Conditions on the Morphology, Crystallinity, and Thermal Stability of Cellulose Nanocrystals Extracted from Kenaf Bast Fibers. *Cellulose* **2012**, *19*, 855−866.

(25) Lin, N.; Dufresne, A. Surface Chemistry, Morphological Analysis and Properties of Cellulose Nanocrystals with Gradiented Sulfation Degrees. *Nanoscale* **2014**, *6*, 5384−5393.

(26) Borjesson, M.; Sahlin, K.; Bernin, D.; Westman, G. Increased Thermal Stability of Nanocellulose Composites by Functionalization of the Sulfate Groups on Cellulose Nanocrystals with Azetidinium Ions. *J. Appl. Polym. Sci.* **2018**, *135*, 45963.

(27) Yoo, Y.; Youngblood, J. P. Green One-Pot Synthesis of Surface Hydrophobized Cellulose Nanocrystals in Aqueous Medium. *ACS Sustainable Chem. Eng.* **2016**, *4*, 3927−3938.

(28) Peng, S. X.; Chang, H.; Kumar, S.; Moon, R. J.; Youngblood, J. P. A Comparative Guide to Controlled Hydrophobization of Cellulose Nanocrystals via Surface Esterification. *Cellulose* **2016**, *23*, 1825−1846.

(29) Fujisawa, S.; Zhang, J.; Saito, T.; Iwata, T.; Isogai, A. Cellulose Nanofibrils as Templates for the Design of Poly(l-Lactide)-Nucleating Surfaces. *Polymer* **2014**, *55*, 2937−2942.

(30) Kloser, E.; Gray, D. G. Surface Grafting of Cellulose Nanocrystals with Poly(Ethylene Oxide) in Aqueous Media. *Langmuir* **2010**, *26*, 13450−13456.

(31) Gan, L.; Liao, J.; Lin, N.; Hu, C.; Wang, H.; Huang, J. Focus on Gradientwise Control of the Surface Acetylation of Cellulose Nanocrystals to Optimize Mechanical Reinforcement for Hydrophobic Polyester-Based Nanocomposites. *ACS Omega* **2017**, *2*, 4725−4736.

(32) Fujisawa, S.; Saito, T.; Kimura, S.; Iwata, T.; Isogai, A. Surface Engineering of Ultrafine Cellulose Nanofibrils toward Polymer Nanocomposite Materials. *Biomacromolecules* **2013**, *14*, 1541−1546.

(33) Sobkowicz, M. J.; Dorgan, J. R.; Gneshin, K. W.; Herring, A. M.; McKinnon, J. T. Renewable Cellulose Derived Carbon Nanospheres as Nucleating Agents for Polylactide and Polypropylene. *J. Polym. Environ.* **2008**, *16*, 131−140.

(34) Cicero, J. A.; Dorgan, J. R.; Janzen, J.; Garrett, J.; Runt, J.; Lin, J. S. Supramolecular Morphology of Two-Step, Melt-Spun Poly-(Lactic Acid) Fibers. *J. Appl. Polym. Sci.* **2002**, *86*, 2828−2838.

(35) Spinella, S.; Lo Re, G.; Liu, B.; Dorgan, J.; Habibi, Y.; Leclere, P.; Raquez, J. M.; Dubois, P.; Gross, R. A. Polylactide/Cellulose Nanocrystal Nanocomposites: Efficient Routes for Nanofiber Modification and Effects of Nanofiber Chemistry on PLA Reinforcement. *Polymer* **2015**, *65*, 9−17.

(36) Ding, W.; Jahani, D.; Chang, E.; Alemdar, A.; Park, C. B.; Sain, M. Development of PLA/Cellulosic Fiber Composite Foams Using Injection Molding: Crystallization and Foaming Behaviors. *Composites, Part A* **2016**, *83*, 130−139.

(37) Chieng, B. W.; Ibrahim, N. A.; Yunus, W. M. Z. W.; Hussein, M. Z. Plasticized Poly(Lactic Acid) with Low Molecular Weight

DOI: 10.1021/acsapm.8b00030
ACS Appl. Polym. Mater. 2019, 1, 160−168

Poly(Ethylene Glycol): Mechanical, Thermal and Morphology Properties. *J. Appl. Polym. Sci.* **2013**, *130*, 4576−4580.
(38) Sungsanit, K.; Kao, N.; Bhattacharya, S. N. Properties of Linear Poly(Lactic Acid)/Polyethylene Glycol Blends. *Polym. Eng. Sci.* **2012**, *52*, 108−116.
(39) Urena-Benavides, E. E.; Kitchens, C. L. Wide-Angle X-Ray Diffraction of Cellulose Nanocrystal-Alginate Nanocomposite Fibers. *Macromolecules* **2011**, *44*, 3478−3484.
(40) Peng, J.; Ellingham, T.; Sabo, R.; Turng, L. S.; Clemons, C. M. Short Cellulose Nanofibrils as Reinforcement in Polyvinyl Alcohol Fiber. *Cellulose* **2014**, *21*, 4287−4298.
(41) Diaz, J. A.; Ye, Z.; Wu, X.; Moore, A. L.; Moon, R. J.; Martini, A.; Boday, D. J.; Youngblood, J. P. Thermal Conductivity in Nanostructured Films: From Single Cellulose Nanocrystals to Bulk Films. *Biomacromolecules* **2014**, *15*, 4096−4101.
(42) Chowdhury, R. A.; Peng, S. X.; Youngblood, J. Improved Order Parameter (Alignment) Determination in Cellulose Nanocrystal (CNC) Films by a Simple Optical Birefringence Method. *Cellulose* **2017**, *24*, 1957−1970.
(43) Read, B. E.; Duncan, J. C.; Meyer, D. E. Birefringence Techniques for the Assessment of Orientation. *Polym. Test.* **1984**, *4*, 143−164.
(44) Alexander, L.. *X-Ray Diffraction Methods in Polymer Science*; Krieger Publishing Co.: Huntington, NY, 1979.
(45) Hermans, J. J.; Hermans, P. H.; Vermaas, D.; Weidinger, A. Quantitative Evaluation of Orientation in Cellulose Fibres From the X-Ray Pibre Diagram. *Recl. des Trav. Chim. des Pays-Bas* **1946**, *65*, 427−447.
(46) Fambri, L.; Pegoretti, A.; Fenner, R.; Incardona, S. D.; Migliaresi, C. Biodegradable Fibres of Poly(l-Lactic Acid) Produced by Melt Spinning. *Polymer* **1997**, *38*, 79−85.
(47) Mathew, A. P.; Oksman, K.; Sain, M. The Effect of Morphology and Chemical Characteristics of Cellulose Reinforcements on the Crystallinity of Polylactic Acid. *J. Appl. Polym. Sci.* **2006**, *101*, 300−310.
(48) Peng, S. X.; Shrestha, S.; Youngblood, J. P. Crystal Structure Transformation and Induction of Shear Banding in Polyamide 11 by Surface Modi Fi Ed Cellulose Nanocrystals. *Polymer* **2017**, *114*, 88−102.

DOI: 10.1021/acsapm.8b00030
ACS Appl. Polym. Mater. 2019, 1, 160−168